

A study of speed ratio affecting the performance of a contra-rotating axial compressor

Y-Y Chen*, B Liu, Y Xuan, and X-R Xiang

School of Engines and Energy, Northwestern Polytechnical University, Xi'an, People's Republic of China

The manuscript was received on 9 April 2008 and was accepted after revision for publication on 21 July 2008.

DOI: 10.1243/09544100JAERO364

Abstract: The performance and detailed flow structure of a counter-rotating compressor under different rotating speed and typical working condition were experimentally and numerically investigated. Numerical results preliminarily showed that the total pressure ratio performance agreed well with experimental data, when the calculated peak efficiency was a little bigger than the experimental one. With optimized speed ratio, the peak isentropic efficiency can be increased with minor reduction of the total pressure ratio and safe margin. Flow reversal first occurred at the start section of the outlet guide vane and it covered nearly 40 per cent area of the whole flow at the stall point when the rotational speed ratio of rotor 1 and rotor 2 were greater than or equal to 1, and it caused the compressor operate in the stall point. First, however, the flow separation and great range low-energy flow occurred at the 30 per cent span range of s rotor blade-tip near stall point, which was the main reason for the compressor stall when the speed ratio is less than 1. Rotor 2 worked at a greater incidence angle because of the separation at the trailing edge of rotor 1.

Keywords: counter-rotating technique, compressor, performance curve, experiment investigation

1 INTRODUCTION

For the development of aviation, the performance requirements of the aero-engine have become much stricter. Current trends in the development of fuel-efficient propulsion systems for air breathing engines point towards the application of contra-rotation either in a pusher undusted fan or in a high bypass ducted fan in up-to-date engines [1]. Over the past years, institutes all over the world have committed themselves to develop high-performance engines, and have obtained some wonderful products, such as the F-119 engines produced by the PW Company, and the Trent-900 engines produced by the Rolls-Royce Company. Both of them have favorable performance and contra-rotating turbine. However, the contra-rotating compressor is singularly seen in the world.

Contra-rotating or rotation of rotors in opposite directions is one of the promising approaches for substantial improvement in aerodynamic performance of an axial flow compressor/fan stage. The stator vanes could be cancelled from the compressor by using contra-rotating technique. Accordingly, the size of the engine could be decreased, and thrust weight ratio of it could be significantly increased. Furthermore, the aircraft resultant moment, caused by the rotating engine shaft, could be decreased obviously by using contra-rotating technique. Then the performance and stability of aircraft could be improved greatly, so that it is significant in the research of contra-rotating compressor.

Some studies on contra-rotating axial flow fans have earlier been reported by Young [2]. The work of Young refers to contra-rotating having equal speeds. In that work, a fan stage comprising of contra-rotors was shown to deliver higher pressure-rise and to provide it through flow capacity. The off-design performance and stalling behaviour of contra-rotors were not, however, explored in that work. In an earlier work of

*Corresponding author: School of Engines and Energy, Northwestern Polytechnic University, Xi'an 710072, People's Republic of China. email: 42627219@mail.nwpu.edu.cn

Nath [3], the stalling behaviour of contra-rotating axial compressor stage was shown that depended upon the speed ratio of the two rotors [3]. It was shown that a significant improvement in stall free range could be obtained by contra-rotating the second rotor at a speed of 50 per cent faster than the first rotor exhibited a completely stall-free characteristic, thus providing an improved aerodynamic performance of the stage. Sharma *et al.* [4] has also reported the effect of various factors on the performance of a contra-rotating compressor stage. To illustrate further the effect of parameters, such as speed ratio and axial gap between the rotors, flow structure details are investigated to examine the performance changes associated with a contra-rotating compressor stage. Sharma and Pundit [5] have done some studies on a single stage axial compressor, with a hub-tip ratio of 0.66. The fastest

rotor speed was 2500 r/min. Few experiments have been done to investigate the factors, such as speed ratio of the two rotors, rotor stagger, pitch-chord ratio, and axial spacing between the rotors, which can affect the performance of a contra-rotating axial compressor. Some research institutions in China have also done some deep investigations in the area of contra-rotating turbines, and have accomplished certain achievements [6–8]. Over the past three years we have done some research on the contra-rotating axial compressor [9, 10].

In this work, the numerical simulation and experimental study have been utilized to obtain the performance characteristics and flow detail of a contra-rotating axial compressor, under huge successful calculation cases of the axial compressor [11, 12]. And optimization analysis is used for rotating speed ratio,

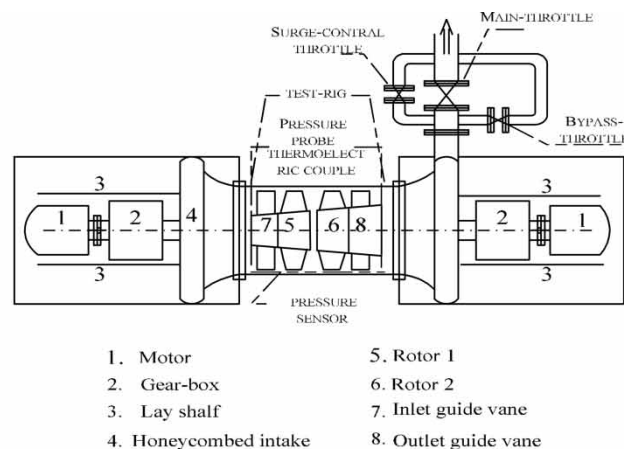


Fig. 1 View of the test compressor: (a) schematic; (b) photograph

which is not only very helpful for better matching between first rotor and second rotor, but also for the increase of efficiency, the reduction of the specific fuel consumption, and increasing the thrust-weight ratio of engines.

2 TEST RIG AND MEASUREMENT TECHNIQUE

The test compressor used for this study is a single-stage contra-rotating axial flow compressor test rigged at the Northwestern Polytechnical University as shown in Fig. 1. Rotor 1 (R1) has 19 blades, with a hub-to-tip ratio of 0.61 and rotor 2 (R2) has 20 blades, with a hub-to-tip ratio of 0.63. For all sets of simulations, the running tip clearance set to be about 0.5 per cent span. The two rotors are driven by two thirster controlled AC motors, respectively, and can be run at any speed combination from 0 to 8000 r/min. The air enters into the inlet filter box by an annular intake and is discharged to the atmosphere through three disc throttle valves installed at the end of the discharge duct.

The compressor total pressure ratio of design is 1.22 at a mass flow of 6.4 kg/s and at 8000 r/min. Rotor performance is usually measured in terms of its total pressure ratio, isentropic efficiency, and mass flow. The flowrate through the compressor is measured from the calibrated pressure rise and temperature difference at the compressor inlet and the outlet. The probe measurements are corrected for Mach number and streamline slope based on a calibration of each probe used and on the design streamline slope. Radial distributions of total temperature are mass averaged across the annulus and of total pressure are energy averaged by converting them to their enthalpy equivalents and then to mass averaged across the annulus. A pressure tap containing a small Kiltie fast response pressure transducer has been positioned behind the rotor to detect the onset of rotating stall. The temperature rise is derived from the thermoelectric couple.

3 DESCRIPTION OF THE NUMERICAL MODEL

Three-dimensional flow computations were carried out with the help of the commercial code EURANUS. This code is an integral part of the software package NUMECA FINE [13]. The numerical method used in the study is outlined as follows.

The Favre–Reynolds averaged Navier–Stokes equations are discretized using a cell-centred explicit finite volume scheme according to Jameson *et al.* [14] in a relative coordinate system rotating together with the reference frame. The steady-state flow solution is achieved at the convergence of a 4-stage explicit Runge–Kutta integration scheme. In this work, the single equation turbulence model of Spalart–Allmaras

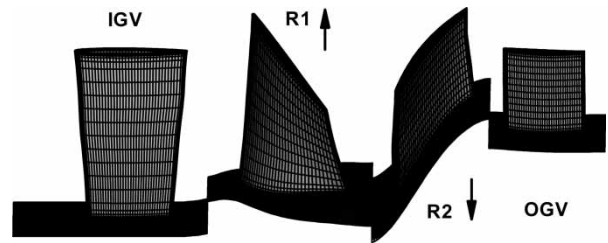


Fig. 2 Three dimension grid of the contra-rotating compressor

(1992) is used to estimate the eddy viscosity. The discretized equations are solved with local time stepping, implicit residual smoothing, and multi-grid techniques to reduce the computational cost.

A composite grid system with structured grids was used to simulate the contra-rotating compressor flow field. Figure 2 shows the three-dimensional computational grid map. The body-fitted C grid topology is applied to all the blades while the simple H-type grid topology is used for the main flow region, and butterfly grid is used at the tip clearance. There are 41 points in the span wise direction, about 250 000 grid points for each blade. The whole computational grid nodes for the contra-rotating compressor are of approximately 1 000 000. To evaluate properly the viscous fluxes at the walls using the chosen boundary conditions (no-slip, adiabatic wall condition without a wall function method), the distance of the first node away from the wall has to be judiciously determined. This becomes an important grid parameter. In this work, the maximum distance between the wall and the first node is set to satisfy that y^+ is equal to or smaller than 2.

4 NUMERICAL RESULTS AND DISCUSSION

The calculated performance curves at 100, 90, 80, and 70 per cent design speeds and the experimental data are shown in Figs 3 and 4. It can be found that near design conditions, the total pressure ratio is in good agreement with measured results, while isentropic efficiency is a little bigger than measurement. CFD results and experimental data indicate that, at off-design speeds, the operation range is narrow with the rotate speed decreasing. In the experiment, isentropic efficiency is gained from the total pressure rise and total temperature difference at the compressor inlet and outlet. Because of the thermoelectric couple, it is difficult to get an exact total temperature rise in the test. For the above reason, there is a little error of efficiency in the experiment data. As shown in Fig. 4, the experiment efficiency has been often oscillated in a little amplitude even when the compressor operates at a fixed condition in its 'stable' region. It is difficult to get an exact efficiency for a compressor in an experiment.

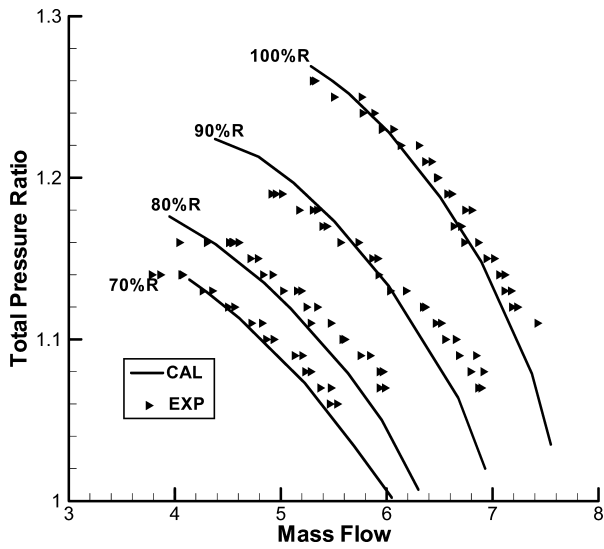


Fig. 3 The calculated and experimental curves of the total pressure ratio at design rotational speed

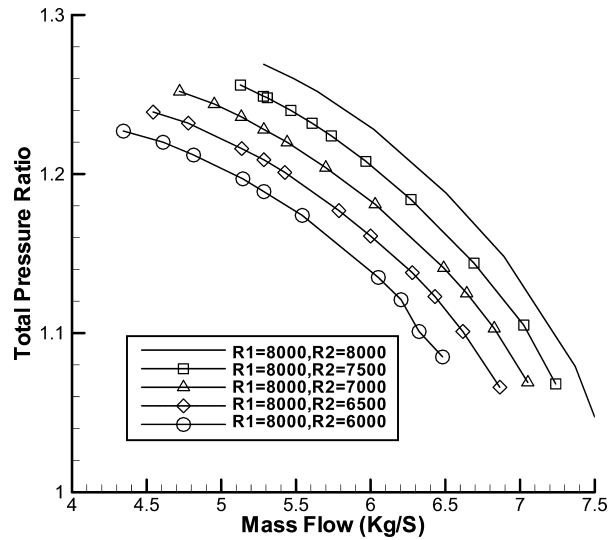


Fig. 5 Total pressure ratio curve at different rotational speed ratio ($\gamma > 1$)

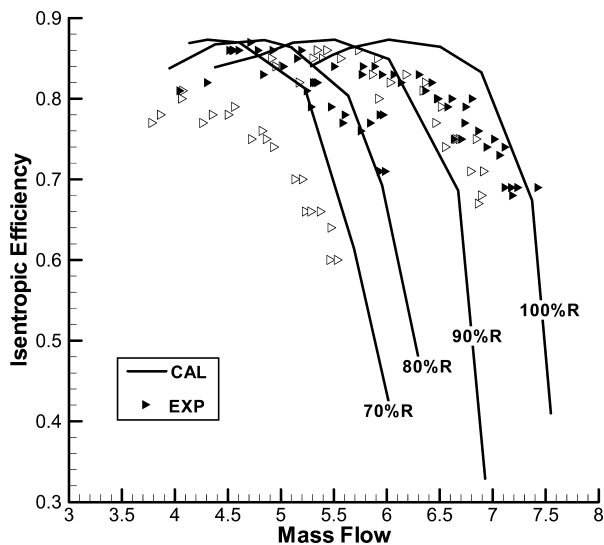


Fig. 4 The calculated and experimental curves of the efficiency at design rotational speed

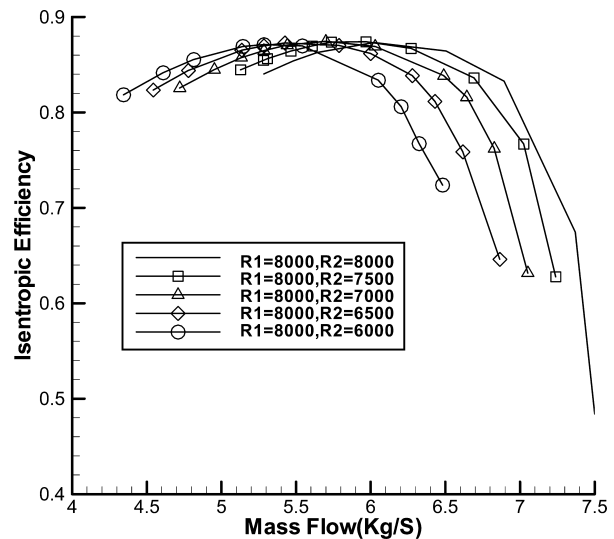


Fig. 6 Isentropic efficiency curve at different rotational speed ratio ($\gamma > 1$)

The effects of the different speed ratio of R1 and R2 were investigated by applying it to a contra-rotating compressor. The overall performance of the compressor with different speed ratio (γ) is shown in Figs 5 to 8. It can be found that the peak total pressure ratio is reduced with the speed ratio (γ) decreasing when $\gamma > 1$, while the isentropic efficiency is different to the total pressure ratio. The peak efficiency was 87.44 per cent when $\gamma = 8/7$, and it was reduced again with the slowing down of R2. The safe margin of mass flow was retained at a comparatively stable region, with the speed ratio playing down when $\gamma > 1$.

Figures 7 and 8 give the performance curves at different speed ratio ($\gamma < 1$). We can see from the graph

that the peak total pressure ratio plays down quickly with R1 speed reduced. This means that in the contra-rotating compressor most work is actualized by R1. The peak efficiency was 87.27 per cent at $\gamma = 7.5/8$ in the range of $\gamma < 1$. The mass flow at choking conditions was oscillated in small amplitude, while the safe margin was decreased.

The peak efficiency of the contra-rotating compressor is shown in Table 1. From Table 1 it is clear that at the design rotational speed the efficiency η_2 was much lower than the efficiency η_1 . The results confirmed that decreasing the R2 speed had a favorable impact on the compressor efficiency. However, in terms of R1 isentropic efficiency, it is harmful when slowing down the R1. From all the above, we could find

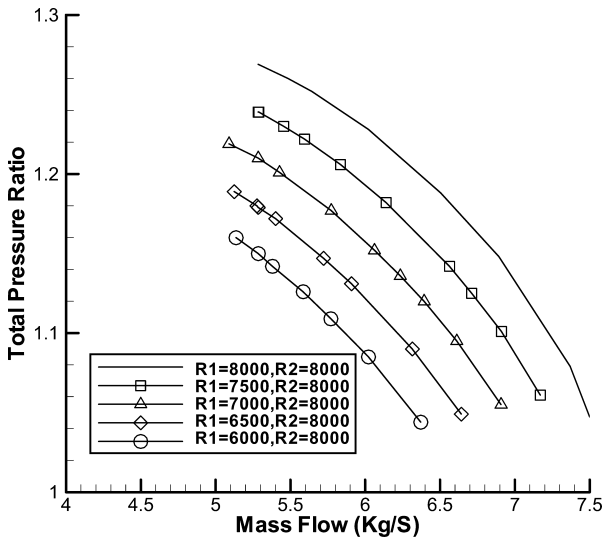


Fig. 7 Total pressure ratio curve at different rotational speed ratio ($\gamma < 1$)

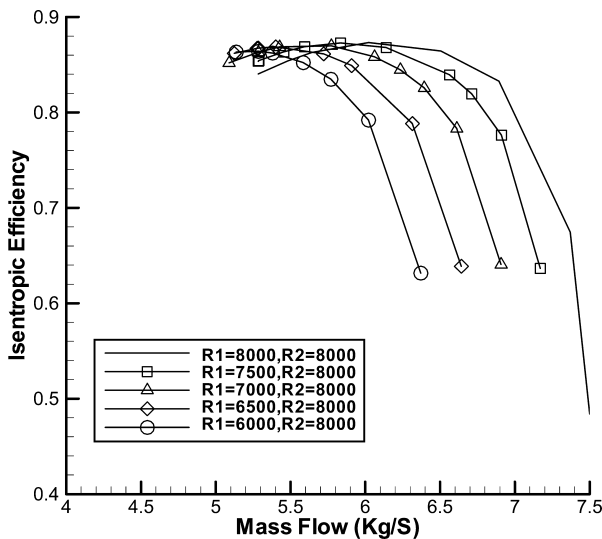


Fig. 8 Isentropic efficiency curve at different rotational speed ratio ($\gamma < 1$)

that if the first rotor is contra-rotated faster than the second rotor the stall margin and the peak pressure ratio are remained, and when R1 is contra-rotated at 1500 r/min faster than R2 the compressor has a peak isentropic efficiency.

Figures 9 and 10 show the flow angle and the blade angle at different rotating ratio choking point. As revealed in Fig. 9, the best incidence angle was achieved at the design rotating speed. When the second rotor was slower by 2000 r/min than the first rotor, there was a greater incidence angle of 5° at the R1 inlet. However, for the second rotor, the biggest incidence angle was achieved when the R2 was faster by 2000 r/min than R1. The incidence angle is one of the main reasons that can cause the compressor to surge.

Table 1 The peak isentropic efficiency (η, η_1, η_2) of the compressor

Speed combination (r/min)	Peak isentropic efficiency (η)	R1 isentropic at efficiency peak point (η_1)	R2 isentropic at efficiency peak point (η_2)
8000–8000	0.8627	0.923 374	0.820 437
8000–7500	0.8741	0.922 241	0.831 48
8000–7000	0.8744	0.924 071	0.824 005
8000–6500	0.8728	0.922 328	0.815 77
8000–6000	0.8710	0.921 97	0.800 784
7500–8000	0.8727	0.919 09	0.843 249
7000–8000	0.8698	0.910 623	0.846 933
6500–8000	0.8687	0.909 61	0.850 381
6000–8000	0.8640	0.895 349	0.852 709

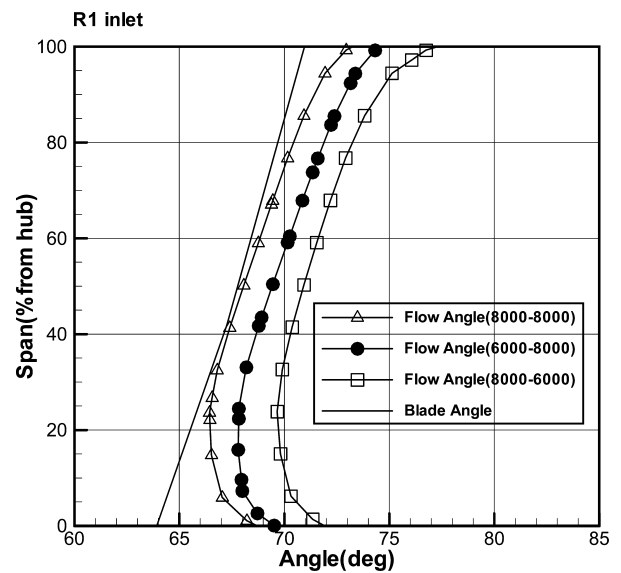


Fig. 9 Flow angle and blade angle of the first rotor at different rotating speed choking point

This means that the big incidence angle of R2 inlet may be the primary reason for the compressor surge.

During the course of compressor surge study, a simple but effective tool for examining the effect of the treatment on the tip leakage flow and its resultant vortex was used to circumferentially average the final predicted flow-field, and to examine the predicted axisymmetric flow velocity vectors near the tip of the rotor [15, 16]. In order to understand the physics that underpin the performance variations shown in Figs 9 and 10, the results should be compared under the same reference state. The relative Mach number contours and streamlines at 98 per cent span section near stall point at different rotating speed ratios are shown in Figs 11 to 13.

From the three pictures, it can be found that R2 was working in a big incidence angle condition. Mach numbers of the peaks are all less than 1.0. Mach number distribution in the pictures indicates that there is no remarkable shock in the flow area. It can be found that the flow reversal first occurs at the start section

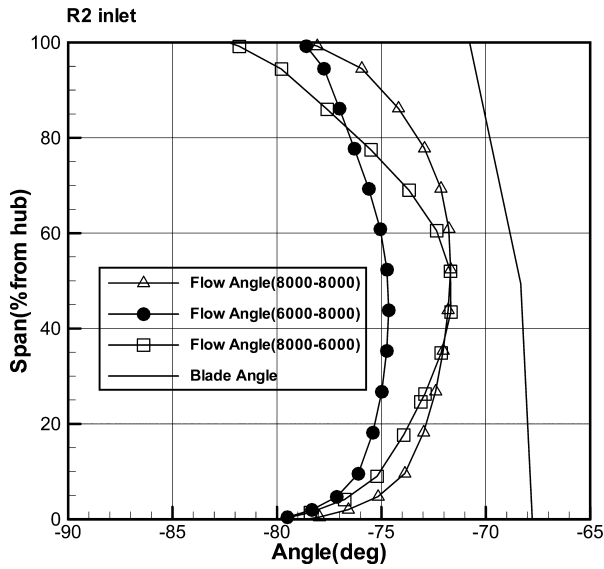


Fig. 10 Flow angle and blade angle of the second rotor at different rotating speed choking point

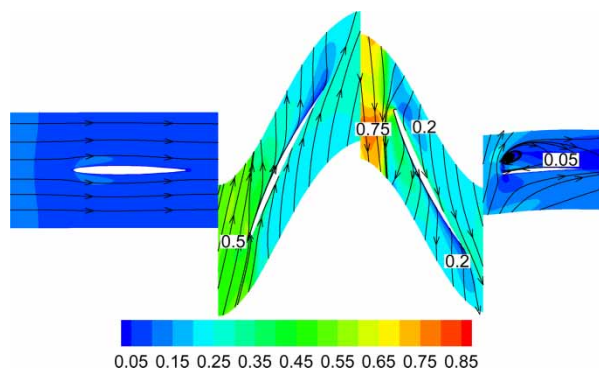


Fig. 11 Relative Mach number contours and stream lines at 98 per cent span section near stall point at the rotating speed ratio of 8000/8000

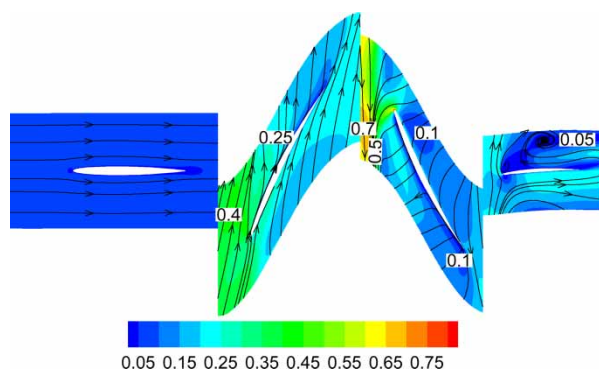


Fig. 12 Relative Mach number contours and stream lines at 98 per cent span section near stall point at the rotating speed ratio of 6000/8000

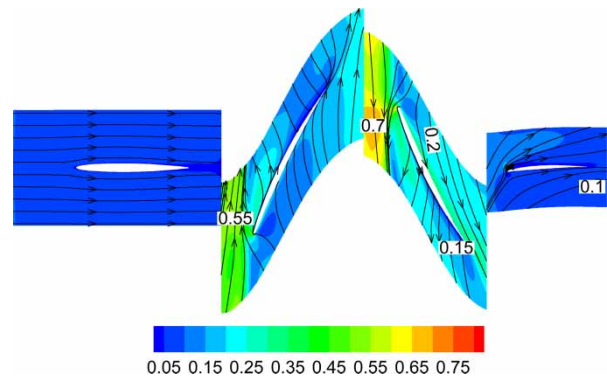


Fig. 13 Relative Mach number contours and stream lines at 98 per cent span section near stall point at the rotating speed ratio of 8000/6000

of the outlet guide vane and it covers nearly 40 per cent area of the whole flow at the stall point with $\gamma = 1$. However, the vortex was separated into two vortices and the covered area increased to 50 per cent of the whole flow when $\gamma = 0.75$. It disappeared when $\gamma = 1.5$. The relative Mach number contours of the pictures show that there is a big area of low Mach number about 0.1 at the middle section of the first rotor when $\gamma = 1.5$. First, the flow separation and great range low energy flow occur at the 30 per cent span range of the first rotor blade tip near the stall point, which is the main reason for the compressor stall. This means that the surge possibly initiates in the outlet guide vane when $\gamma \geq 1$ while it may occur in the first rotor section when $\gamma < 1$.

5 CONCLUSIONS

The performances and flow field in a contra-rotating axial flow compressor at design and off design conditions were investigated by computations and experiments in this article. One goal of this investigation was to discuss the dissimilitude between contra-rotating compressor and general compressor. The other goal of this research was to make some understanding of the physical processes occurring when the compressor approaches the stall, and the mechanism of how the different rotating speed ratios influence the stall margin and the compressor performance. Detailed discussions of the study would be helpful to understand the rotor/rotor interaction mechanisms between R1 and R2 at 98 per cent span with different rotating speeds. Based on the simulations and tests the following conclusions are drawn:

1. The steady time averaged results show reasonable agreement with the experimental data. Because of the cancelled stator vanes, contra-rotating compressor's operating margin is smaller than general compressor.

2. The contra-rotating compressor's performance in different speed combinations of R1 and R2 indicates that the speed ratio between two rotors significantly affects the off-design performance of both the two rotors and the stage. The contra-stage with speed ratio of 1.143 has been found to attain a higher efficiency with minor reduction of the total pressure ratio and operating margin. Whereas, a smaller stable stall free operating range is achieved when the speed ratio less than 1 ($\gamma \leq 1$) and the range decreases with the speed ratio reduction.
3. The flow structure at the tip section of the contra-rotating compressor has been found to vary with speed ratio between R1 and R2. Detailed discussion of flow interactions at the tip section of the contra-stage with different speed ratios show that the surge possibly initiates at the outlet guide vane when $\gamma \geq 1$, whereas it may occur at the first rotor section when $\gamma \leq 1$. The details of the flow visualization at the tip have exposed the different flow vortex topologies in the outlet guide vane with different rotating speeds.
4. The future investigations will concentrate on the question of how the flow at the tip section has to be directed in order to increase flow stability and efficiency as much as possible.

REFERENCES

- 1 Schimming, P. Counter rotating fans: an aircraft propulsion for the future. *J. Therm. Sci.*, 2003, **12**(2), 97–103.
- 2 Young, R. H. Contra-rotating axial fans. *J. Inst. Heat. Vent. Eng.*, 1951, **18**, 187.
- 3 Nath, G. Non-free vortex flow in contra-rotating axial-rotating fans. *Ind. J. Technol.*, 1969, **7**, 379–385.
- 4 Sharma, P. B., Jain, Y. P., Jha, N. K., and Khanna, B. B. Stalling behaviour of a contra-rotating axial compressor stage. ISABE paper 85-7087, 1985.
- 5 Sharma, P. B. and Pundir, D. S. A study of some factors affecting the performance of a contra-rotating axial compressor stage. In the 8th ISABE Conference, Cincinnati, June 1987, ISABE paper 87-7038.
- 6 Wang, H., Zhao, Q., Zhao, X., and Xu, J. Unsteady numerical simulation of shock systems in vaneless counter-rotating turbine. In the ASME Turbo Expo 2005, Reno, Nevada, USA, ASME paper GT2005-68212.
- 7 Ji, L., Chen, J., Huang, H., and Xu, J. The key techniques in utilizing vane less counter-rotating turbine. *J. Eng. Thermophys.*, 2003, **24**(1), 35–38.
- 8 Ji, L., Chen, J., Huang, H., and Xu, J. Investigation about effects of axial gap on the performance of vaneless counter-rotating turbine. *J. Eng. Thermophys.*, 2002, **23**(5), 565–568.
- 9 Liu, B., Yang, Y., Wang, Y., and Chen, Y. Investigation of influence of rotational speed and pressure ratio on performance of two-stage counter-rotating compressor. *J. Northwest. Polytech. Univ.*, 2007, **25**(4), 576–580.
- 10 Wang, Y., Liu, B., Chen, Y., and Jiang, J. Flow field investigation of dual stage counter-rotating compressor. *J. Northwest. Polytech. Univ.*, 2006, **24**(1), 97–100.
- 11 Lu, X. G., Chu, W. L., Wu, Y. H., and Zhu, J. Q. Mechanism of the interaction between casing treatment and tip leakage flow in a subsonic axial compressor. In the ASME Turbo Expo 2006, Barcelona, Spain, 2006, ASME paper GT-2006-90077.
- 12 Chen, Y., Liu, B., Cao, Z., and Ma, C. Flow field and performance investigation of an axial-centrifugal combined compressor. *J. Propuls. Technol.*, 2007, **28**(4), 356–361.
- 13 NUMECA's flow integrated environment for turbo machinery and internal flows. User manual version 6.1-1, April 2003.
- 14 Jameson, A., Schmit, W., and Turkel, E. Numerical solution of the Euler equations by finite volume methods using Runge-Kutta time-stepping schemes. In the AIAA 14th Fluid and Plasma Dynamic Conference, California, June 1981, AIAA paper 81-1259.
- 15 Lu, X., Chu, W., Zhu, J., and Wu, Y. Experimental and numerical investigation of a subsonic compressor with bend skewed slot casing treatment. In the ASME Turbo Expo, Barcelona, Spain, 2006, ASME paper GT-2006-90026.
- 16 Lu, X., Zhu, J., Chu, W., and Wang, R. The effects of stepped tip gap on performance and flowfield of a subsonic axial-flow compressor rotor. In the ASME Turbo Expo 2005, Reno, Nevada, USA, ASME paper GT-2005-69106.

APPENDIX

Notation

R1	first rotor
R2	second rotor
γ	R1 rotating speed/R2 rotating speed
η	isentropic efficiency of the compressor
η_1	isentropic efficiency of the first rotor and inlet guide vane
η_2	isentropic efficiency of the second rotor and outlet guide vane